

# Quantum dot lasers for silicon photonics [Invited]

Alan Y. Liu,<sup>1,\*</sup> Sudharsanan Srinivasan,<sup>2</sup> Justin Norman,<sup>1</sup> Arthur C. Gossard,<sup>1,2</sup> and John E. Bowers<sup>1,2</sup>

<sup>1</sup>Materials Department, University of California Santa Barbara, Santa Barbara, California 93106, USA

<sup>2</sup>Department of Electrical and Computer Engineering, University of California Santa Barbara, Santa Barbara, California 93106, USA

\*Corresponding author: ayliu01@engineering.ucsb.edu

Received April 3, 2015; revised May 20, 2015; accepted May 21, 2015;  
posted June 4, 2015 (Doc. ID 235818); published July 15, 2015

We review recent advances in the field of quantum dot lasers on silicon. A summary of device performance, reliability, and comparison with similar quantum well lasers grown on silicon will be presented. We consider the possibility of scalable, low size, weight, and power nanolasers grown on silicon enabled by quantum dot active regions for future short-reach silicon photonics interconnects. © 2015 Chinese Laser Press

OCIS codes: (140.5960) Semiconductor lasers; (250.0250) Optoelectronics.  
<http://dx.doi.org/10.1364/PRJ.3.0000B1>

## 1. INTRODUCTION

To circumvent inefficient light emission from silicon, current methods to fabricate silicon-based lasers typically utilize gain from separate material. These methods include wafer bonding or direct growth of III–V materials onto silicon or silicon-on-insulator (SOI) substrates, as well as band engineering of group IV elements such as Ge or GeSn for direct gap light emission [1–4]. Direct growth of high-gain III–V laser material onto large area, low-cost silicon substrates is well suited for high-volume applications. Unfortunately, large dislocation densities result from the growth process due to fundamental material differences between III–V compound semiconductors and silicon, which are detrimental to laser performance and reliability [5]. A primary focus of III–V growth on silicon, therefore, has been to minimize the number of generated dislocations as much as possible. Despite significant reductions in dislocation density to  $10^5$ – $10^6$  cm<sup>-2</sup>, dislocation densities near native substrate levels ( $10^3$  cm<sup>-2</sup>) appear difficult to achieve in planar bulk layers.

Substituting quantum dot active regions in place of quantum wells can further mitigate the negative effect of residual dislocations on laser performance. Efficient capture and 3D confinement of injected carriers by the individual quantum dots leads to reduced nonradiative recombination at defects or dislocations [6,7]. As a result, the effect of dislocations still present in the active layer is greatly diluted by the total number of dots, which are independent of each other. A quantum dot laser epitaxially grown on silicon was first reported more than 15 years ago [8]. Since then, various other device demonstrations have been reported with continued improvement in device performance [9–15].

Here, we review various approaches to integrate InAs/GaAs quantum dot lasers for silicon photonics applications, focusing on direct epitaxial growth. In addition, we present a direct comparison of quantum dot versus quantum well lasers epitaxially grown on silicon to demonstrate the effectiveness of quantum dot active regions in mitigating the negative effects associated with residual dislocations. Looking forward, we consider the possibility of quantum-dot-based III–V

nanolasers epitaxially grown on silicon or SOI substrates as a scalable light source capable of meeting the reduced size, weight, and power (SWaP) requirements for future high-bandwidth-density, short-reach optical links [16].

## 2. RECENT PROGRESS IN QUANTUM DOT LASERS FOR SILICON PHOTONICS

InAs/GaAs self-assembled quantum dot lasers are the most well-studied semiconductor quantum dot system and will be the primary focus of this section. They are an attractive light source to meet low-power consumption and athermal performance demands for silicon photonics devices, having demonstrated the lowest threshold current densities and highest lasing temperatures of any telecom laser [17,18]. We review various methods to integrate such lasers for silicon photonics applications in the sections below, with focus given to direct epitaxial growth of quantum dot lasers onto silicon substrates.

### A. External Coupling

One approach, which is ready for immediate commercial adoption, is integration of quantum dot lasers via flip-chip bonding and butt coupling to “silicon optical interposer” chips consisting of spot size converters, optical modulators, photodetectors, and power splitters. Transceivers made with these components demonstrated error-free operation (bit-error-rate <math>10^{-12}</math>) at 20 Gbps per channel from 25°C to 125°C without active adjustment of the modulator or photodiode across this temperature range [19]. With a footprint of 0.106 mm<sup>2</sup> per channel, this translates to a bandwidth density of 19 Tbps/cm<sup>2</sup>. Externally coupled quantum dot comb lasers—to be used as a highly efficient temperature stable light source in conjunction with silicon microring modulators for dense wavelength division multiplexing—have also been proposed [20,21].

### B. Wafer Bonding

InAs/GaAs quantum dot lasers on silicon have also been made by wafer bonding. Using direct fusion bonding at 300°C–500°C, broad area lasers (2.1 mm × 100 μm) with direct

current injection across the bonded GaAs/Si interface show pulsed lasing thresholds of  $205 \text{ A/cm}^2$  [22]. A pulsed lasing temperature up to  $110^\circ\text{C}$  was reported by bonding p-doped InAs/GaAs quantum dot lasers in a later report [23]. The previous structures were bonded onto bulk silicon substrates; however, wafer-bonded quantum dot lasers on SOI substrates with etched waveguides have also been demonstrated, paving the way for future integration with hybrid silicon photonic integrated circuit technology [24].

Metal mediated bonding has also been explored to fabricate similar laser structures. A recent demonstration using this approach reported an InAs quantum dot ridge laser on SOI ( $2 \text{ mm} \times 5 \text{ }\mu\text{m}$  with a  $2 \text{ }\mu\text{m}$  wide current channel) by metal stripe bonding with a room-temperature pulsed threshold of  $110 \text{ mA}$  [25]. Polymer adhesive bonding is another commonly used bonding technique [2]. Although quantum dot lasers adhesively bonded to silicon have not yet been reported, the realization of such a device should be straightforward.

### C. Direct Growth

Direct growth of quantum dot lasers onto silicon or SOI substrates represents another exciting approach to build light sources on silicon. Historically, this approach has been limited by the generation of dislocations from the heteroepitaxial growth process, which acts as shunt paths as well as optical absorption centers within the laser structure. By using a quantum dot active region with a dot density much greater than the dislocation density, the former effect can be significantly reduced via efficient capture and spatial confinement of injected carriers by individual quantum dots.

The first  $1.3 \text{ }\mu\text{m}$  quantum dot laser epitaxially grown on silicon was reported in 2011 by direct nucleation of GaAs onto vicinal silicon substrates [12]. Using  $\text{In}_{0.15}\text{Ga}_{0.85}\text{As}/\text{GaAs}$  strained layer superlattice dislocation filter layers, room-temperature-pulsed lasing was achieved in a cleaved facet broad area laser ( $3 \text{ mm} \times 50 \text{ }\mu\text{m}$ ) with a threshold current density of  $725 \text{ A/cm}^2$  and  $26 \text{ mW}$  of output power. Lasing was limited up to  $42^\circ\text{C}$ . In this case, the bottom contact was on the silicon substrate with current injected across the GaAs/Si interface.

More recently, by substituting  $\text{In}_{0.15}\text{Al}_{0.85}\text{As}/\text{GaAs}$  in place of  $\text{In}_{0.15}\text{Ga}_{0.85}\text{As}/\text{GaAs}$  strained layer superlattices for improved dislocation filtering, as well as employing a top-top contact geometry to avoid current injection through the dislocated GaAs/Si interface, the pulsed lasing threshold for a  $3 \text{ mm} \times 25 \text{ }\mu\text{m}$  broad area laser was reduced to  $200 \text{ A/cm}^2$ . The maximum pulsed lasing temperature was elevated to  $111^\circ\text{C}$  with more than  $100 \text{ mW}$  of output power obtained from a single cleaved facet [14]. Continuous-wave (CW) performance was not reported for this device.

Previously, CW lasing of InAs/GaAs quantum dot lasers grown on a germanium substrate was demonstrated with comparable performance to the same laser structure on GaAs substrates [26]. Epitaxial growth of germanium on silicon is a mature CMOS technology, and Ge/Si templates are now widely available commercially. Since Ge is nearly lattice matched to GaAs ( $0.08\%$  lattice mismatch), growth of GaAs on Ge/Si substrates allows for decoupling of the lattice mismatch and polarity mismatch issues into separate interfaces. The first room-temperature CW lasing of InAs/GaAs quantum dot lasers epitaxially grown on silicon was achieved using

such an intermediate Ge buffer approach [13]. This structure exhibited very low room temperature pulsed lasing thresholds of  $64 \text{ A/cm}^2$  as well as room-temperature CW lasing thresholds of  $163 \text{ A/cm}^2$ . Maximum CW output power at room temperature was  $3.7 \text{ mW}$  from both facets for a  $3.5 \text{ mm} \times 20 \text{ }\mu\text{m}$  cavity. CW lasing was sustained up to  $30^\circ\text{C}$  in a separate  $3 \text{ mm}$  long device.

Improved CW performance was reported for a similar structure grown on Ge/Si substrates using a higher number of active region quantum dot layers for increased modal gain, narrow-ridge waveguide geometries, and high-reflection coatings [15]. Room-temperature CW thresholds as low as  $16 \text{ mA}$ , output powers up to  $176 \text{ mW}$ , and lasing up to  $119^\circ\text{C}$  were reported from such devices.  $T_0$  values between  $100\text{--}200 \text{ K}$  were achieved by modulation p-doping the GaAs barriers in the active region, which is an established technique for improving the thermal performance of InAs/GaAs quantum dot lasers [27]. Repeatability was demonstrated between two separate wafers, showing a reasonably uniform threshold current density distribution over 330 different devices, with an average of threshold current density of  $500 \text{ A/cm}^2$  and as low as  $250 \text{ A/cm}^2$ .

A representative summary of quantum dot lasers directly grown on silicon is presented in Table 1, illustrating the rapid improvement in various key device metrics in recent years. The emission wavelength of such lasers have been between  $1$  and  $1.3 \text{ }\mu\text{m}$ . Another wavelength of interest for optical interconnects is around  $1.55 \text{ }\mu\text{m}$ . InAs quantum dot lasers on III-V substrates have been demonstrated at this wavelength using either metamorphic InGaAs buffers on GaAs or InAs/InP-based quantum dots [28,29]. In principle, realization of  $1.55 \text{ }\mu\text{m}$  InAs quantum dot lasers on silicon by epitaxial growth should be possible as long as the quantum dot nature of the active region and its associated benefits are preserved.

## 3. QUANTUM DOT VERSUS QUANTUM WELL LASERS EPITAXIALLY GROWN ON SILICON

The prospect of using quantum dots to reduce the effect of dislocations was proposed as early as 1991 [6]. Recently reported results of In(Ga)As quantum dot lasers epitaxially grown on silicon substrates seems to support the hypothesis that quantum dot ensembles are less sensitive to dislocations compared to quantum wells [11–15]. However, a direct comparison of the two grown on silicon with similar dislocation densities are lacking, not allowing for the separation of this effect from other factors that may contribute to good laser performance such as low dislocation density, growth, or processing differences. Here, we present direct comparison of the optical properties of In(Ga)As quantum dot versus quantum well emitters grown on GaAs and silicon substrates to assess this hypothesis. The growth, processing, and measurement techniques in this study were identical except for the usage of either quantum dots or quantum wells for the active region.

### A. Experimental Procedures

$\text{In}_{0.20}\text{Ga}_{0.80}\text{As}/\text{GaAs}$  quantum well lasers emitting around  $980 \text{ nm}$  are among the most mature laser systems on GaAs and were chosen for this study to compare with  $1.3 \text{ }\mu\text{m}$  InAs/GaAs quantum dot lasers. The following cases are examined:

**Table 1. Representative Summary of In(Ga)As/GaAs Self-Assembled Quantum Dot Lasers Epitaxially Grown on Silicon**

Year	$I_{th}$ (mA)/ $J_{th}$ (A cm <sup>-2</sup> )	Max Lasing Temp (°C)	Device Size (μm <sup>2</sup> )	$\lambda$ (μm)	Ref.
1999	788/3850 (Pulsed 80 K)	—	800 × 50	1 (80 K)	[8]
2005–2009	500/900 (Pulsed)	95 (Pulsed)	600 × 80 (lowest threshold), 800 × 8 (highest temperature)	1	[9–11]
2011	1087.5/725 (Pulsed)	42 (Pulsed)	3000 × 50	1.3	[12]
2012	45/64.3 (Pulsed), 114/163 (CW)	84 (Pulsed), 30 (CW)	3500 × 20 (lowest threshold), 3000 × 20 (highest temperature)	1.26	[13]
2014	150/200 (Pulsed)	111 (Pulsed)	3000 × 25	1.25	[14]
2014	16/430 (CW)	119 (CW), >130 (Pulsed)	(700–1200) × (4–12)	1.25	[15]

- InGaAs quantum well lasers versus InAs quantum dot lasers on native GaAs substrates (dislocation density  $\leq 10^3$  cm<sup>-2</sup>)
- InGaAs quantum well lasers on silicon versus InAs quantum dot lasers on silicon (dislocation density  $\geq 10^8$  cm<sup>-2</sup>)

Photoluminescence (PL) and full laser structures are studied. Growth was performed by molecular beam epitaxy (MBE). The PL structures consist of a single quantum well or quantum dot active region cladded on either side by GaAs (50 nm)/Al<sub>0.40</sub>Ga<sub>0.60</sub>As (50 nm)/GaAs (50 nm). Growth procedures for the quantum dots have been previously reported [30]. Growth conditions for the quantum well are 8 nm of In<sub>0.20</sub>Ga<sub>0.80</sub>As grown at 2.23 Å/s, 530°C, and under a V/III ratio of 20.

GaAs/Al<sub>x</sub>Ga<sub>1-x</sub>As laser structures were grown with either  $3 \times [\text{In}_{0.20}\text{Ga}_{0.8}\text{As}(8 \text{ nm})/\text{GaAs}(8 \text{ nm})]$  multiple quantum wells, or InAs quantum dot/GaAs (37.5 nm) multiple quantum dot layers (five for lasers on GaAs and seven for lasers on silicon) (see Fig. 1). Samples on GaAs were grown on cleaved pieces of a semi-insulating 2-in. GaAs (100) wafer, and samples on silicon were grown on 2 cm × 2 cm pieces diced from a 150 mm GaAs (1 μm)-on-Ge (500 nm)-on-Si template provided by IQE. The silicon wafer was (100) with a 6° miscut toward [111] to suppress the formation of antiphase domains. The as-grown epi were then processed into either broad-area or narrow-ridge waveguide lasers using standard lithography, dry etching, and metallization techniques.

## B. Results and Discussion

50-μm-wide broad-area lasers with as-cleaved facets were first fabricated from the GaAs wafers to assess the quality of the

300 nm GaAs:Be ( $2 \times 10^{19}$ cm <sup>-3</sup> )
50 nm 40 → 0% Al <sub>x</sub> Ga <sub>(1-x)</sub> As:Be ( $1 \times 10^{19}$ cm <sup>-3</sup> )
1.4 μm Al <sub>0.4</sub> Ga <sub>0.6</sub> As:Be cladding ( $7 \times 10^{17}$ cm <sup>-3</sup> )
20 nm 20 → 40% Al <sub>x</sub> Ga <sub>(1-x)</sub> As:Be ( $4 \times 10^{17}$ cm <sup>-3</sup> )
30 nm Al <sub>0.2</sub> Ga <sub>0.8</sub> As:Be SCH ( $4 \times 10^{17}$ cm <sup>-3</sup> )
50 nm GaAs
QW or QD active region
50 nm GaAs
30 nm Al <sub>0.2</sub> Ga <sub>0.8</sub> As:Si SCH ( $2 \times 10^{17}$ cm <sup>-3</sup> )
20 nm 40 → 20% Al <sub>x</sub> Ga <sub>(1-x)</sub> As:Si ( $2 \times 10^{17}$ cm <sup>-3</sup> )
1.4 μm Al <sub>0.4</sub> Ga <sub>0.6</sub> As:Si cladding ( $2 \times 10^{17}$ cm <sup>-3</sup> )
50 nm 0 → 40% Al <sub>x</sub> Ga <sub>(1-x)</sub> As:Si ( $1 \times 10^{18}$ cm <sup>-3</sup> )
2000 nm GaAs:Si ( $2 \times 10^{18}$ cm <sup>-3</sup> )
1000 nm GaAs:UID
500 nm Ge:UID
Si (100) 6° → [111]

Fig. 1. Layer structure of the quantum well or quantum dot GaAs/AlGaAs lasers on silicon. QW: quantum well; QD: quantum dot.

active region. For each type of laser (quantum dot or quantum well), the light-versus-current (LI) characteristics for lasers with various cleaved cavity lengths were measured on over 100 devices. Injection efficiency ( $\eta_i$ ) and optical loss ( $\alpha_i$ ) were extracted from the best-fit line of the average inverse differential efficiency versus the cavity length. Pulsed measurements with a duty cycle of 0.5% (5 μs pulse width, 1000 μs pulse period) were used for this analysis, although CW measurements were also performed with quantum well and quantum dot lasers demonstrating good performance at room temperature. Subsequently, a modal gain ( $\Gamma g_{th} = \frac{1}{L} \ln \frac{1}{0.30} + \alpha_i$ ) versus current density curve was generated by plotting the modal gain versus average threshold current density of each different cavity length. These results are summarized in Fig. 2. We see that in low-loss cavities, quantum dots hold a significant advantage in terms of lower transparency and threshold current density.

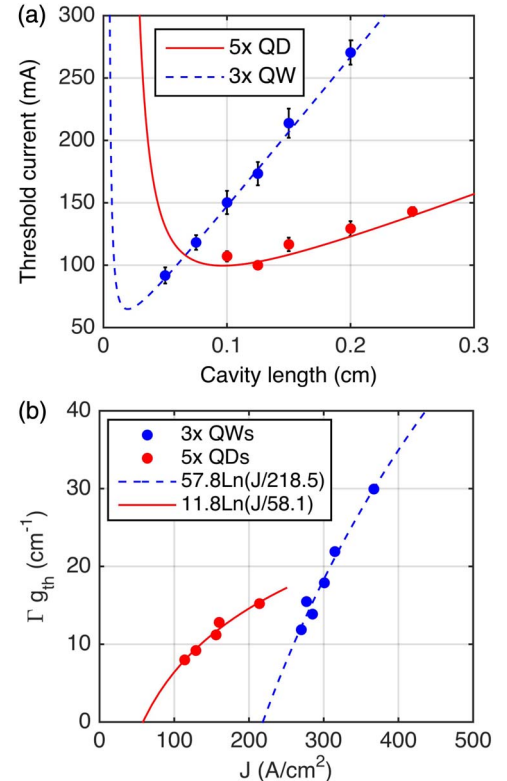


Fig. 2. Room-temperature broad-area laser characteristics of In<sub>0.2</sub>Ga<sub>0.8</sub>As quantum well and InAs quantum dot lasers on GaAs substrates. (a) Threshold current versus cavity length. (b) Modal gain versus injected current density. Fitting parameters are listed in Table 2.

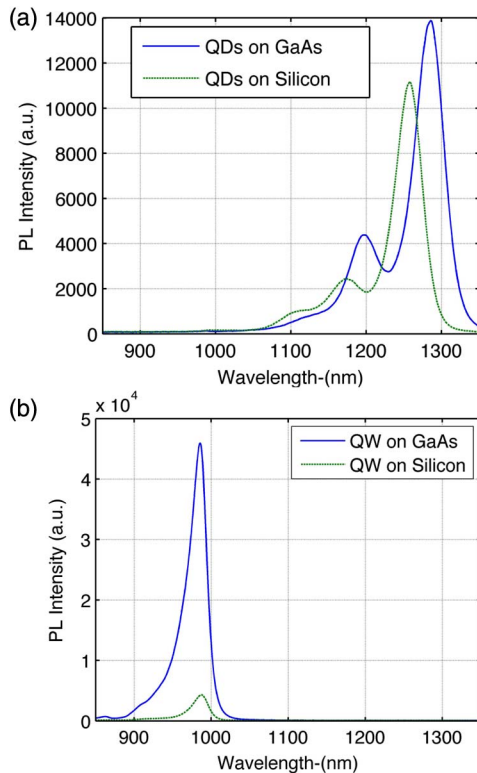


Fig. 3. Room-temperature PL comparison of (a) single InAs quantum dot layer and (b) single 8 nm  $\text{In}_{0.20}\text{Ga}_{0.80}\text{As}$  quantum well grown on GaAs versus silicon substrates.

Room-temperature PL spectra of the same quantum well or quantum dot structure grown on GaAs versus silicon is shown in Fig. 3. While the ground-state intensity of the quantum well degraded by more than a factor of 10 when grown on silicon, the ground-state intensity of the InAs quantum dots is roughly 80% of the reference quantum dots grown on GaAs with comparable linewidths ( $\sim 35$  meV).

Ridge waveguide lasers were fabricated from the two different kinds of laser epi on silicon using the same fabrication procedure. Cross-sectional transmission electron microscopy (TEM) images of the quantum dot and quantum well laser structures grown on silicon are shown in Fig. 4. Similar dislocation densities are observed for both structures; thus, we may infer that the dislocation densities in the PL structures grown on silicon are also comparable (since the substrates were all diced from the same parent wafer).

Contact resistance from devices on the two separate wafers were similar at around  $1 \times 10^{-6} \Omega \text{cm}^2$ , as to be expected, since doping levels were nominally identical, and the metallization procedures were the same. I-V characteristics between devices from the two separate wafers also show similar series resistance [Figs. 5(a) and 5(b)]. However, contrary to the case of the two lasers on GaAs substrates, in this case none of the quantum well devices were able to achieve CW lasing at room temperature [Fig. 5(c)]. In comparison, the InAs quantum dot lasers grown on silicon show reasonable CW lasing characteristics, as shown in Fig. 5(d) and reported in detail in [15]. The turn-on voltage of the quantum well lasers is also lower than what would be expected from the bandgap of the quantum wells, indicating possible current leakage. These results

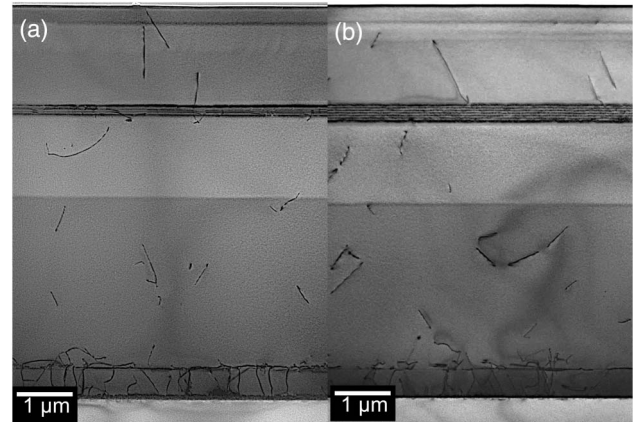


Fig. 4. Bright-field cross-sectional TEM images of (a) quantum well laser and (b) quantum dot laser grown on silicon. Dislocations manifest as irregular dark lines. (Scale is approximate.)

clearly show that quantum dot lasers can be much less sensitive to dislocations compared with quantum wells.

#### 4. RELIABILITY OF QUANTUM DOT LASERS DIRECTLY GROWN ON SILICON

Other groups have reported good performance of quantum well lasers epitaxially grown on silicon substrates through sufficient reductions in dislocation density [31–33]. However, the reliability of such lasers remains a concern, particularly for GaAs-based lasers, which are susceptible to recombination-enhanced defect reactions [5,34]. The longest reported lifetime for a GaAs-based quantum well laser epitaxially grown on silicon is around 200 h at room temperature [31].

We have studied the reliability of several InAs/GaAs quantum dot lasers grown on silicon aged at  $30^\circ\text{C}$  under constant current stress at 100 mA [35]. No catastrophic failures were observed, and threshold versus aging time plots typically followed a sublinear increase versus aging time. Measured time to failure, defined as the time required to double the initial threshold, ranged from 260 to 2783 h. Plan-view TEM images of aged and unaged devices revealed that the dislocation density in the active region was  $10^8 \text{cm}^{-2}$  in both cases, with misfit dislocations in the aged devices acquiring a helical component, which is characteristic of dislocation climb [36].

Figure 6 shows the results of a reliability study for one of our quantum dot lasers. This particular laser has a projected mean time to failure of 4600 h and surpassed 2100 h of CW operation at  $30^\circ\text{C}$  under an applied current density of  $2 \text{kA/cm}^2$  before the aging process was stopped for characterization. The fairly long operating lifetimes possible, despite the very high dislocation densities, are likely due to a combination of the efficient carrier capture and radiative recombination within individual quantum dots competing against the nonradiative carrier trapping at dislocations as well as a possible precipitate hardening effect from the high strain field surrounding individual quantum dots [37,38].

Although these lifetimes fall short of typical reliability requirements for commercial use, the dislocation densities in these structures are still around two orders of magnitude higher than the state of the art III-Vs grown on silicon [35]. Further, the quantum dot active region stands to benefit from additional improvements in dot uniformity and/or increasing

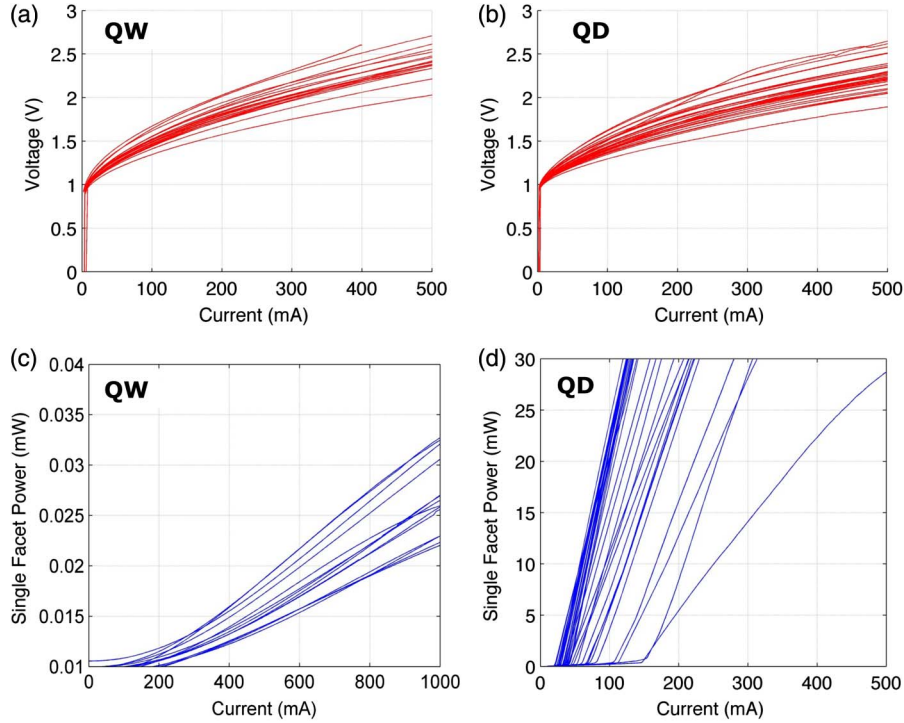


Fig. 5. (a) and (b) Room-temperature CW current–voltage and (c) and (d) light-versus-current plots for the (a) and (c) In<sub>0.20</sub>Ga<sub>0.80</sub>As quantum well and (b) and (d) InAs quantum dot lasers grown on silicon substrates.

dot density. The combination of such improvements of the quantum dot active region and dislocation reduction is expected to produce reliable devices in the future.

## 5. QUANTUM DOT NANOLASERS ON SILICON

Significant reductions in size, cost, and power consumption of optical interconnects are desirable to facilitate their implementation in high-volume short-reach communication links (i.e., chip to chip or shorter) [16]. Here, we consider the possibility of quantum-dot-enabled nanolasers epitaxially grown on silicon as a low-cost, low-SWaP light source in silicon photonic integrated circuits to meet these requirements. Such nanolasers would contain one (or multiple) layers of a high-uniformity ensemble of III–V quantum dots embedded in a low-loss cavity a few tens of square micrometers in area grown on silicon. A quantum-dot-based nanolaser configuration on silicon presents several advantages:

- The combination of a low-transparency current density quantum dot active region with a miniaturized low-loss cavity

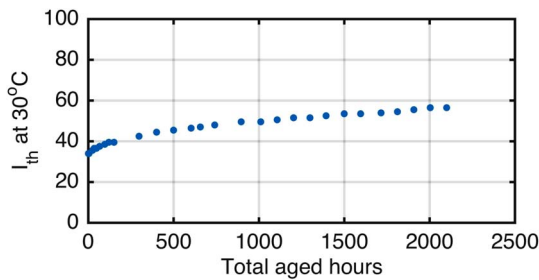


Fig. 6. Threshold current at the aging temperature of 30°C versus total aging time in hours for one of the InAs quantum dot lasers epitaxially grown on Ge/Si substrates reported in [15].

can produce the very low lasing thresholds necessary for low power consumption optical links (see Fig. 7).

- By limiting the total device area to tens of square micrometers or less, epitaxial necking and dislocation image forces can facilitate dislocation glide out of the crystal side-walls, and the total dislocation count within the active layers can be very low [39,40]. The use of a quantum dot active region is expected to further mitigate any negative effects from residual dislocations, as was demonstrated above in Section 2.

- The small form factors of these devices also lend themselves to higher on-chip integration densities, favorable from an energy efficiency perspective to minimize interfacial coupling losses and signal attenuation, and necessary to achieve high interconnect bandwidth density [16,41].

- Epitaxial growth will allow this technology to scale with the largest available silicon wafer size, taking advantage of economies of scale not available for III–V substrates. Changing from a continuous planar epi coverage to limited-area epitaxy in this case reduces the total amount of accumulated thermal stress in accordance with the reduced epi filling factor, which can mitigate wafer yield issues due to thermal-stress-induced cracking [42].

In the sections below, we examine various technical aspects of the proposed structure in detail.

### A. Waveguide Coupling

Figure 8 shows one approach to achieve waveguide coupling where the optical mode is butt-coupled to a silicon rib waveguide. In this embodiment, the III–V cavity is selectively grown onto the handle wafer of a SOI substrate, and the height of the active region is aligned with the silicon waveguide layer to maximize optical coupling. The handle wafer can serve as a contact layer as well as an excellent heat sink for the III–V

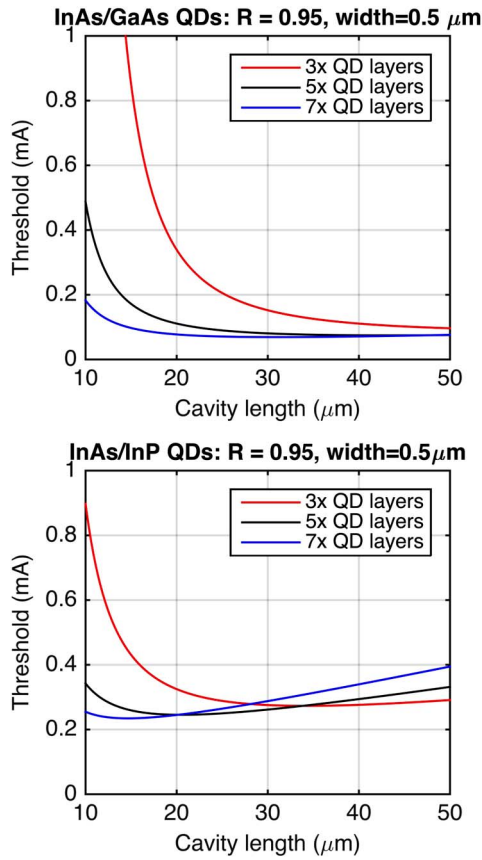


Fig. 7. Scaled broad-area laser threshold currents versus cavity length for GaAs- and InP-based quantum dots. A facet reflectivity  $R = 95\%$  was assumed for both cases. Gain parameters used are listed in Table 2.

layers. Figure 9 shows the calculated profile of the fundamental transverse electric (TE) mode for an InAs/InP quantum dot nanolaser stack side by side with a silicon rib waveguide with a partial etch depth of 250 nm and a total waveguide height of 500 nm. In this case, the maximum coupling efficiency is computed to be 92.35% ( $\sim 0.35$  dB coupling loss). The etch depth of the partially etched silicon layers may be varied to tailor the transverse mode profile of the III-V and

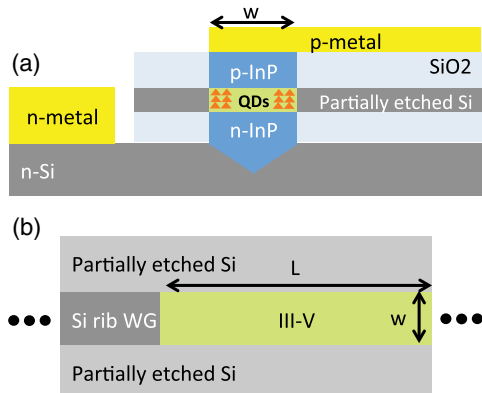


Fig. 8. (a) Transverse cross-sectional schematic of the proposed quantum dot nanolaser where the output is butt-coupled to an Si rib waveguide (WG). (b) Top-down view of the active region plane. The active region is aligned to the thicker Si rib waveguide to maximize coupling, while the partial etch depth can be varied to tailor the transverse index profile. A calculated mode profile is shown in Fig 9.

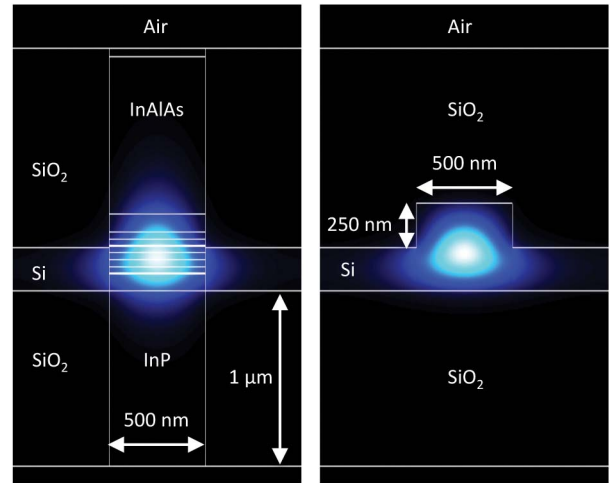


Fig. 9. Calculated fundamental TE mode profiles of an InAs/InP quantum dot nanolaser on SOI with seven quantum dot layers (left) and a half-etched Si rib waveguide to which the laser may be butt-coupled to (right). The estimated coupling loss is  $\sim 0.35$  dB. The confinement factor for the quantum dot layers is  $\sim 1.95\%$ . The depth of the partially etched Si layers may be varied to tailor the transverse index/mode profile to maximize coupling.

silicon waveguide sections to further optimize the coupling efficiency.

### B. High-Reflectivity Mirrors

High mirror reflectivity is crucial in reducing mirror loss of short cavity lasers. Quantum dot lasers also will have a distinct advantage over quantum well lasers in terms of energy efficiency if the total cavity loss is low enough to allow for operation near the transparency current density, which will be inherently lower in quantum dot systems compared to quantum wells (see Fig. 2). Possible approaches to reduce mirror loss include high-quality factor ( $Q$ ) ring cavities, Bragg reflectors (distributed feedback or distributed bragg reflectors), dielectric mirrors, and metallic mirrors. Figure 10 shows a schematic for the various types of mirrors.

Bragg reflectors are a preferable choice for obtaining high reflectivity with low loss, where the reflection strength can be tailored by the etch depth and number of grating periods. In our proposed structure, the Bragg reflectors can be realized by etching gratings in the silicon waveguide or as distributed feedback gratings in the upper cladding layer [see Fig. 10(a) and 10(b)]. First-order Bragg gratings require high-precision lithography and etching. Higher-order gratings may simplify fabrication but at the expense of some excess mirror loss due to variations in duty cycle.

Metallic mirrors can provide polarization and wavelength independent reflection with relatively simple fabrication. However, the material loss limits the reflection to  $\sim 97.5\%$  [43]. Two metal plugs deposited on either side of the laser can form a high- $Q$  resonator [Fig. 10(c)], and the light can be coupled out using a directional coupler parallel to the active region, as described in [43]. A combination of metal mirror on one side and a Bragg mirror on the other also can be used for unidirectional output. High-reflection metal or dielectric facet coatings are also an option but would have limited applicability for on-chip light sources.

High- $Q$  ring cavities may be used to achieve low cavity loss in place of conventional Fabry-Perot cavities. In this

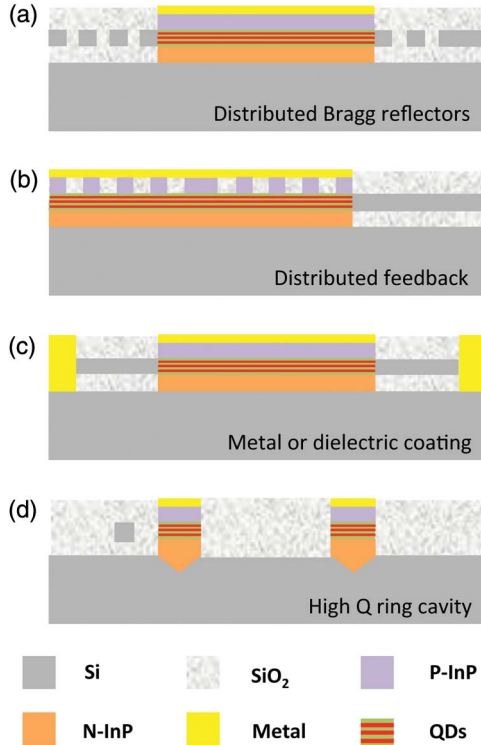


Fig. 10. Schematic of the longitudinal cross section for an InAs/InP quantum dot nanolaser showing different possible mirror designs. (a) Distributed Bragg reflector mirrors in silicon. (b) Distributed feedback gratings. (c) Metal or dielectric high-reflection coatings. (d) High- $Q$  ring cavity coupled to an output waveguide (shown on the left traveling perpendicular to the page).

configuration, light from a whispering gallery mode circulating inside the ring cavity can be coupled to a nearby silicon waveguide, as shown in Fig. 10(d). Additional reflectors can be defined on one end of the silicon waveguide to achieve unidirectional lasing, as described in [44].

### C. Surface Recombination

Surface recombination can be a dominant factor in determining device performance and reliability of small devices. Improved lateral carrier confinement in quantum dots with respect to quantum wells is yet another compelling reason to employ quantum dots for nanolasers, which can significantly reduce the surface recombination current compared to quantum wells [45,46]. We have examined the impact of surface recombination on the scaling of the broad-area threshold current for InAs/GaAs quantum dots and InAs/InP quantum dots. We follow the approach outlined in [46], where it was shown that InAs/GaAs quantum dot lasers have an order of magnitude lower surface recombination velocities and  $\sim 5\times$  shorter mean am-bipolar diffusion lengths compared with InGaAs/GaAs quantum well lasers. In these calculations, a simple rectangular fully etched mesa was assumed. From simulations of various waveguide geometries, the lateral TE mode cutoff is around  $0.5\ \mu\text{m}$ , which we took for a lower bound ridge width in the calculations. Changes in lateral confinement versus ridge width was accounted for via the effective index method, although the magnitude of the variation versus width was not large ( $\sim 5\%$  reduction at a width of  $0.5\ \mu\text{m}$ ).

Different parameters and assumptions used are listed in Table 2. Results are shown in Fig. 11. Although the overall

**Table 2. Parameters Used for Calculations in Figs. 7 and 11<sup>a</sup>**

	InAs/GaAs	InAs/InP
$v_s$ (cm/s)	$5 \times 10^4$	$1 \times 10^4$
$\tau$ (ns)	2.8	2.8
$\alpha_i$ ( $\text{cm}^{-1}$ )	3.16	4
$J_{br}$ ( $\text{A}/\text{cm}^2$ )	11.6	39
$\eta_i$	0.6	0.26
$\Gamma g_{0J}$ ( $\text{cm}^{-1}$ per layer)	2.36	5
$R$	0.95	0.95

<sup>a</sup>Gain and loss values are from Fig. 2 for InAs/GaAs quantum dots and [29] for InAs/InP quantum dots. Recombination velocities and carrier lifetimes are from [46,48].

threshold of GaAs-based quantum dots is lower, the threshold at a ridge width of  $0.5\ \mu\text{m}$  and, assuming an am-bipolar diffusion length of  $1\ \mu\text{m}$  is  $5.88\times$  the scaled broad-area laser threshold, whereas InP-based quantum dots show a  $2.08\times$  increase due to the lower surface recombination velocity. Despite the high surface recombination current at submicrometer scales, very low thresholds are still achievable. If the optical properties of InAs/InP quantum dots can be improved to the level of InAs/GaAs quantum dots, they may be a superior material system for nanolasers due to the reduced surface recombination velocity. Various surface treatments and passivation techniques may be used to further reduce the surface trap density and the surface recombination velocity [47–49].

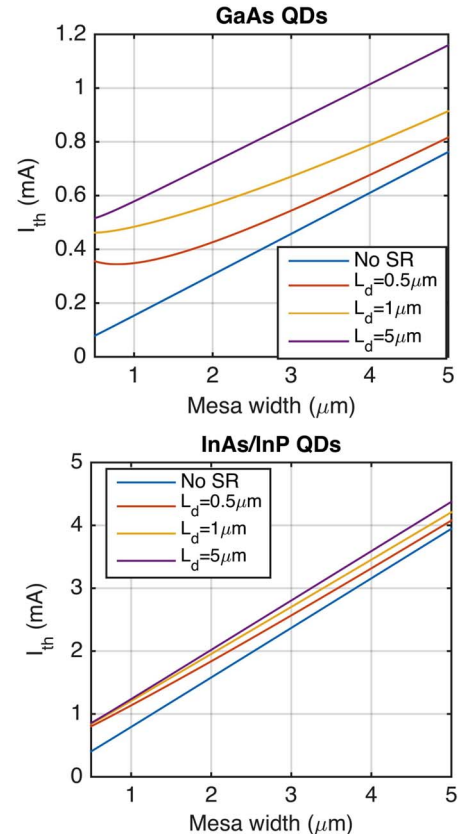


Fig. 11. Calculated threshold currents versus ridge width for both GaAs ( $v_s = 5 \times 10^4$  cm/s) and InP ( $v_s = 1 \times 10^4$  cm/s) quantum dots and various diffusion lengths. A mean diffusion length of  $1\ \mu\text{m}$  was reported in [46]. A cavity length of  $50\ \mu\text{m}$ ,  $R = 95\%$ , and seven quantum dot layers were assumed for both cases (see Table 2).

## 6. CONCLUSION

We have reviewed recent advances of quantum dot lasers for silicon photonics, focusing on direct epitaxial growth onto silicon. Comparison of quantum dot versus quantum well lasers grown on silicon clearly demonstrates the advantage of using quantum dot active regions. High-temperature, high-power, and low-threshold operation has been demonstrated with quantum dot lasers directly grown on silicon. Over 2700 h of CW operation has been achieved with such structures, which is the longest lifetime of any GaAs-based lasers grown on silicon. Quantum-dot-based nanolasers directly grown on silicon are interesting candidates as scalable, low-SWaP light sources for future short-reach silicon photonic interconnects.

## ACKNOWLEDGMENTS

This work was supported by DARPA MTO E-PHI and the Semiconductor Research Corporation. A. Y. Liu and J. Norman are grateful for the support of NSF graduate research fellowships. The authors thank IQE for supplying the GaAs/Ge/Si substrates.

## REFERENCES

- D. Liang and J. E. Bowers, "Recent progress in lasers on silicon," *Nat. Photonics* **4**, 511–517 (2010).
- G. Roelkens, L. Liu, D. Liang, R. Jones, A. Fang, B. Koch, and J. Bowers, "III-V/silicon photonics for on-chip and intra-chip optical interconnects," *Laser Photon. Rev.* **4**, 751–779 (2010).
- R. E. Camacho-Aguilera, Y. Cai, N. Patel, J. T. Bessette, M. Romagnoli, L. C. Kimerling, and J. Michel, "An electrically pumped germanium laser," *Opt. Express* **20**, 11316–11320 (2012).
- S. Wirths, R. Geiger, N. von den Driesch, G. Mussler, T. Stoica, S. Mantl, Z. Ikonik, M. Luysberg, S. Chiussi, J. Hartmann, H. Sigg, J. Faist, D. Buca, and D. Grutzmacher, "Lasing in direct-bandgap GeSn alloy grown on Si," *Nat. Photonics* **9**, 88–92 (2015).
- O. Ueda and S. J. Pearton, *Materials and Reliability Handbook for Semiconductor Optical and Electron Devices* (Springer, 2013).
- J.-M. Gerard and C. Weisbuch, "Semiconductor structure for optoelectronic components with inclusions," U.S. patent 5,075,742 (December 24, 1991).
- J. Gérard, O. Cabrol, and B. Sermage, "InAs quantum boxes: highly efficient radiative traps for light emitting devices on Si," *Appl. Phys. Lett.* **68**, 3123–3125 (1996).
- K. Linder, J. Phillips, O. Qasaimeh, X. Liu, S. Krishna, P. Bhattacharya, and J. Jiang, "Self-organized  $\text{In}_{0.4}\text{Ga}_{0.6}\text{As}$  quantum-dot lasers grown on Si substrates," *Appl. Phys. Lett.* **74**, 1355–1357 (1999).
- Z. Mi, P. Bhattacharya, J. Yang, and K. Pipe, "Room-temperature self-organized  $\text{In}_{0.5}\text{Ga}_{0.5}\text{As}$  quantum dot laser on silicon," *Electron. Lett.* **41**, 742–744 (2005).
- J. Yang, P. Bhattacharya, and Z. Mi, "High-performance  $\text{In}_{0.5}\text{Ga}_{0.5}\text{As}$ /GaAs quantum-dot lasers on silicon with multiple-layer quantum-dot dislocation filters," *IEEE Trans. Electron Devices* **54**, 2849–2855 (2007).
- Z. Mi, J. Yang, P. Bhattacharya, G. Qin, and Z. Ma, "High-performance quantum dot lasers and integrated optoelectronics on Si," *Proc. IEEE* **97**, 1239–1249 (2009).
- T. Wang, H. Liu, A. Lee, F. Pozzi, and A. Seeds, "1.3- $\mu\text{m}$  InAs/GaAs quantum-dot lasers monolithically grown on Si substrates," *Opt. Express* **19**, 11381–11386 (2011).
- A. Lee, Q. Jiang, M. Tang, A. Seeds, and H. Liu, "Continuous-wave InAs/GaAs quantum-dot laser diodes monolithically grown on Si substrate with low threshold current densities," *Opt. Express* **20**, 22181–22187 (2012).
- S. Chen, M. Tang, J. Wu, Q. Jiang, V. Dorogan, M. Benamara, Y. Mazur, G. Salamo, A. Seeds, and H. Liu, "1.3  $\mu\text{m}$  InAs/GaAs quantum-dot laser monolithically grown on Si substrates operating over 100°C," *Electron. Lett.* **50**, 1467–1468 (2014).
- A. Y. Liu, C. Zhang, J. Norman, A. Snyder, D. Lubyshev, J. M. Fastenau, A. W. Liu, A. C. Gossard, and J. E. Bowers, "High performance continuous wave 1.3  $\mu\text{m}$  quantum dot lasers on silicon," *Appl. Phys. Lett.* **104**, 041104 (2014).
- D. A. Miller, "Device requirements for optical interconnects to silicon chips," *Proc. IEEE* **97**, 1166–1185 (2009).
- D. Bimberg and U. W. Pohl, "Quantum dots: promises and accomplishments," *Mater. Today* **14**(9), 388–397 (2011).
- T. Kageyama, K. Nishi, M. Yamaguchi, R. Mochida, Y. Maeda, K. Takemasa, Y. Tanaka, T. Yamamoto, M. Sugawara, and Y. Arakawa, "Extremely high temperature (220°C) continuous-wave operation of 1300-nm-range quantum-dot lasers," in *The European Conference on Lasers and Electro-Optics* (Optical Society of America, 2011).
- Y. Urino, N. Hatori, K. Mizutani, T. Usuki, J. Fujikata, K. Yamada, T. Horikawa, T. Nakamura, and Y. Arakawa, "First demonstration of athermal silicon optical interposers with quantum dot lasers operating up to 125°C," *J. Lightwave Technol.* **33**, 1223–1229 (2014).
- D. Livshits, A. Gubenko, S. Mikhlin, V. Mikhlin, C.-H. Chen, M. Fiorentino, and R. Beausoleil, "High efficiency diode comb-laser for DWDM optical interconnects," in *IEEE Optical Interconnects Conference* (2014), pp. 83–84.
- C.-H. J. Chen, T.-C. Huang, D. Livshits, A. Gubenko, S. Mikhlin, V. Mikhlin, M. Fiorentino, and R. Beausoleil, "A comb laser-driven DWDM silicon photonic transmitter with microring modulator for optical interconnect," in *CLEO: Science and Innovations* (Optical Society of America, 2015), paper STu4F-1.
- K. Tanabe, K. Watanabe, and Y. Arakawa, "III-V/Si hybrid photonic devices by direct fusion bonding," *Sci. Rep.* **2**, 349 (2012).
- K. Tanabe, T. Rae, K. Watanabe, and Y. Arakawa, "High-temperature 1.3  $\mu\text{m}$  InAs/GaAs quantum dot lasers on Si substrates fabricated by wafer bonding," *Appl. Phys. Express* **6**, 082703 (2013).
- K. Tanabe and Y. Arakawa, "1.3  $\mu\text{m}$  InAs/GaAs quantum dot lasers on SOI waveguide structures," in *CLEO: Science and Innovations* (Optical Society of America, 2014), paper STh1G-6.
- Y.-H. Jhang, K. Tanabe, S. Iwamoto, and Y. Arakawa, "InAs/GaAs quantum dot lasers on silicon-on-insulator substrates by metal-stripe wafer bonding," *IEEE Photon. Technol. Lett.* **27**, 875–878 (2015).
- H. Liu, T. Wang, Q. Jiang, R. Hogg, F. Tutu, F. Pozzi, and A. Seeds, "Long-wavelength InAs/GaAs quantum-dot laser diode monolithically grown on Ge substrate," *Nat. Photonics* **5**, 416–419 (2011).
- R. R. Alexander, D. T. Childs, H. Agarwal, K. M. Groom, H.-Y. Liu, M. Hopkinson, R. A. Hogg, M. Ishida, T. Yamamoto, M. Sugawara, Y. Arakawa, T. J. Badcock, R. J. Royce, and D. J. Mowbray, "Systematic study of the effects of modulation p-doping on 1.3- $\mu\text{m}$  quantum-dot lasers," *IEEE J. Quantum Electron.* **43**, 1129–1139 (2007).
- L. Y. Karachinsky, T. Kettler, I. Novikov, Y. M. Shernyakov, N. Y. Gordeev, M. Maximov, N. Kryzhanovskaya, A. Zhukov, E. Semenova, A. Vasil'Ev, V. Ustinov, G. Fiol, M. Kuntz, A. Lochmann, O. Schulz, L. Reissmann, K. Posilovic, R. Kovsh, S. Mikhlin, V. Shchukin, N. Ledentsov, and D. Bimberg, "Metamorphic 1.5  $\mu\text{m}$ -range quantum dot lasers on a GaAs substrate," *Semicond. Sci. Technol.* **21**, 691 (2006).
- C. Gilfert, V. Ivanov, N. Oehl, M. Yacob, and J. Reithmaier, "High gain 1.55  $\mu\text{m}$  diode lasers based on InAs quantum dot like active regions," *Appl. Phys. Lett.* **98**, 201102 (2011).
- A. Y. Liu, C. Zhang, A. Snyder, D. Lubyshev, J. M. Fastenau, A. W. Liu, A. C. Gossard, and J. E. Bowers, "MBE growth of P-doped 1.3  $\mu\text{m}$  InAs quantum dot lasers on silicon," *J. Vac. Sci. Technol. B* **32**, 02C108 (2014).
- Z. I. Kazi, P. Thilakan, T. Egawa, M. Umeno, and T. Jimbo, "Realization of GaAs/AlGaAs lasers on Si substrates using epitaxial lateral overgrowth by metalorganic chemical vapor deposition," *Jpn J. Appl. Phys.* **40**, 4903 (2001).
- J. Li, J. Hydrick, J. Park, J. Li, J. Bai, Z. Cheng, M. Carroll, J. Fiorenza, A. Lochtefeld, W. Chan, and Z. Shellenbarger, "Monolithic integration of GaAs/InGaAs lasers on virtual Ge substrates via aspect-ratio trapping," *J. Electrochem. Soc.* **156**, H574–H578 (2009).



33. X. Huang, Y. Song, T. Masuda, D. Jung, and M. Lee, "InGaAs/GaAs quantum well lasers grown on exact GaP/Si (001)," *Electron. Lett.* **50**, 1226–1227 (2014).
34. L. Kimerling, "Recombination enhanced defect reactions," *Solid-State Electron.* **21**, 1391–1401 (1978).
35. A. Liu, R. Herrick, O. Ueda, P. Petroff, A. Gossard, and J. Bowers, "Reliability of InAs/GaAs quantum dot lasers epitaxially grown on silicon," *IEEE J. Sel. Top. Quantum Electron.* **21**, 1900708 (2015).
36. P. Petroff and R. Hartman, "Defect structure introduced during operation of heterojunction GaAs lasers," *Appl. Phys. Lett.* **23**, 469–471 (1973).
37. R. Beanland, A. Sanchez, D. Childs, K. Groom, H. Liu, D. Mowbray, and M. Hopkinson, "Structural analysis of life tested 1.3  $\mu\text{m}$  quantum dot lasers," *J. Appl. Phys.* **103**, 014913 (2008).
38. R. Beanland, J. David, and A. Sanchez, "Quantum dots in strained layers preventing relaxation through the precipitate hardening effect," *J. Appl. Phys.* **104**, 123502 (2008).
39. E. Fitzgerald and N. Chand, "Epitaxial necking in GaAs grown on pre-patterned Si substrates," *J. Electron. Mater.* **20**, 839–853 (1991).
40. X. Zhang, P. Li, G. Zhao, D. W. Parent, F. Jain, and J. Ayers, "Removal of threading dislocations from patterned heteroepitaxial semiconductors by glide to sidewalls," *J. Electron. Mater.* **27**, 1248–1253 (1998).
41. M. J. Heck and J. E. Bowers, "Energy efficient and energy proportional optical interconnects for multi-core processors: driving the need for on-chip sources," *IEEE J. Sel. Top. Quantum Electron.* **20**, 332–343 (2014).
42. A. Able, W. Wegscheider, K. Engl, and J. Zweck, "Growth of crack-free GaN on Si (111) with graded AlGaIn buffer layers," *J. Cryst. Growth* **276**, 415–418 (2005).
43. S. Zamek, L. Feng, M. Khajavikhan, D. T. Tan, M. Ayache, and Y. Fainman, "Micro-resonator with metallic mirrors coupled to a bus waveguide," *Opt. Express* **19**, 2417–2425 (2011).
44. D. Liang, S. Srinivasan, D. Fattal, M. Fiorentino, Z. Huang, D. Spencer, J. Bowers, and R. Beausoleil, "Teardrop reflector-assisted unidirectional hybrid silicon microring lasers," *IEEE Photon. Technol. Lett.* **24**, 1988–1990 (2012).
45. J. K. Kim, R. L. Naone, and L. A. Coldren, "Lateral carrier confinement in miniature lasers using quantum dots," *IEEE J. Sel. Top. Quantum Electron.* **6**, 504–510 (2000).
46. S. A. Moore, L. O'Faolain, M. A. Cataluna, M. B. Flynn, M. V. Kotlyar, and T. F. Krauss, "Reduced surface sidewall recombination and diffusion in quantum-dot lasers," *IEEE Photon. Technol. Lett.* **18**, 1861–1863 (2006).
47. E. Yablonovitch, C. Sandroff, R. Bhat, and T. Gmitter, "Nearly ideal electronic properties of sulfide coated GaAs surfaces," *Appl. Phys. Lett.* **51**, 439–441 (1987).
48. M. Boroditsky, I. Gontijo, M. Jackson, R. Vrijen, E. Yablonovitch, T. Krauss, C.-C. Cheng, A. Scherer, R. Bhat, and M. Krames, "Surface recombination measurements on III-V candidate materials for nanostructure light-emitting diodes," *J. Appl. Phys.* **87**, 3497–3504 (2000).
49. V. Chobpattana, E. Mikheev, J. Y. Zhang, T. E. Mates, and S. Stemmer, "Extremely scaled high-k/ $\text{In}_{0.53}\text{Ga}_{0.47}\text{As}$  gate stacks with low leakage and low interface trap densities," *J. Appl. Phys.* **116**, 124104 (2014).